

Beam Management with Orientation and RSRP using Deep Learning for Beyond 5G Systems

Khuong N. Nguyen, Anum Ali, Jianhua Mo, Boon Loong Ng, Vutha Va, and Jianzhong Charlie Zhang
Standards and Mobility Innovation Laboratory, Samsung Research America, Plano, TX 75023 USA
Email: {k.nguyen1, anum.ali, jianhua.m, b.ng, vutha.va, jianzhong.z}@samsung.com

Abstract—Beam management (BM), i.e., the process of finding and maintaining a suitable transmit and receive beam pair, can be challenging, particularly in highly dynamic scenarios. Side-information, e.g., orientation, from on-board sensors can assist the user equipment (UE) BM. In this work, we use the orientation information coming from the inertial measurement unit (IMU) for effective BM. We use a data-driven strategy that fuses the reference signal received power (RSRP) with orientation information using a recurrent neural network (RNN). Simulation results show that the proposed strategy performs much better than the conventional BM and an orientation-assisted BM strategy that utilizes particle filter in another study. Specifically, the proposed data-driven strategy improves the beam-prediction accuracy up to 34% and increases mean RSRP by up to 4.2 dB when the UE orientation changes quickly.

Index Terms—Beam Management, Sensor-aided Communication, Artificial Intelligence, Deep Learning, Beyond 5G, 6G

I. INTRODUCTION

Communication at millimeter wave (mmWave) and terahertz (THz) frequencies is suitable for high data-rate applications due to the availability of large bandwidth [1], [2]. The use of large antenna arrays with beamforming at the transmitter and receiver is needed to achieve an adequate link margin and to overcome the high free-space path loss [3]. The process of identifying and maintaining a suitable beam pair for the link is known as beam management (BM) [4], [5]. Successful BM is difficult, particularly in the urban area and highly mobile scenarios where the channel changes frequently [6].

Due to the strong fitting ability, machine learning (ML) has been adopted as a promising solution for mmWave beam alignment, which is inherently a complex nonlinear problem. The context information, such as user equipment (UE) locations [7]–[9], sub-6 GHz out-of-band information [10], [11], could be used to predict the best beam. By capturing the temporal correlation of mmWave channels experienced by the mobile UE, the long short-term memory (LSTM) based methods were proposed for beam tracking and proactive beam switching in [12]–[15]. These work, however, did not consider the 3D orientation of a hand-held UE which could rotate quickly in daily usage, e.g., from the portrait to the landscape mode.

In this paper, we use onboard sensor information as additional information to improve performance and achieve efficient BM at the UE. Specifically, we jointly use the orientation information from the inertial measurement unit (IMU) and the reference signal received power (RSRP) for BM. The orientation information is readily available since IMUs are

used in most consumer electronic devices, such as mobile phones, augmented reality (AR)/virtual reality (VR) gadgets, and unmanned aerial vehicles (UAVs). The main contribution of this work is that we developed a method to utilize both RSRP and orientation information to achieve successful BM at the UE with the help of deep learning. The orientation-assisted BM problem is formulated as a classification problem, with RSRP and orientation information as inputs and beam index as output. A recurrent neural network (RNN) is used for classification. The proposed formulation is consistent with 5G new radio (NR) signaling and does not require any modifications to the standard. We present simulation results using a practical UE beam codebook and realistic ray-tracing multi-path channels. These practical assumptions make the evaluation results more credible. Compared to the case without orientation information, the proposed strategy improves beam prediction accuracy by up to 34% and mean RSRP by up to 4.2 dB when the UE rotates quickly.

The remainder of this paper is organized in the following manner. The related work is discussed in the next section. The communication system model, the RSRP, and the orientation model are discussed in Section III. In Section IV, we present the simulation setup that we used to generate the data to train the RNN model. The proposed deep learning based BM strategy is described in detail in Section V. We present numerical results in Section VI to demonstrate the effectiveness of the proposed strategy. Finally, Section VII concludes the paper.

II. RELATED WORK

There has been some previous work on BM [16]–[20] using orientation information. Given the best beam before orientation change and the orientation change, the best beam after orientation change is predicted in [16]. Specifically, first, the angle-of-arrival (AoA) is obtained from the best beam, and then to predict the best beam after orientation change, the change in orientation is converted into a change in AoA. The orientation and position of the UE relative to the base station (BS) are tracked and used for beam steering in [17]. The change in pitch is used to maintain the line-of-sight (LOS) link between two vehicles in [18]. Location and orientation are jointly used in an ML-based inverse fingerprinting method for BM in [19]. Finally, [20] employs a particle filter (PF) to combine the orientation and RSRP information for BM.

The earlier work on using orientation information for BM has several shortcomings. In particular, the strategy of [16] can

work only if the AoA aligns with the best beam's peak, which is not guaranteed. As a result, any prediction based on AoA that is incorrect is also likely to be sub-optimal. The beam steering method of [17], i.e. relative position/orientation tracking, is useful only in LOS. Furthermore, the beam steering ignores the hardware limitations of current mmWave systems. Only in vehicular context, where the leading and following vehicles have a strong LOS path and change in pitch is the primary source of change in the LOS path, is the strategy of [18] useful. Unlike this work, the techniques of [16]–[19] do not take into account the 5G NR signaling and realistic beam codebooks.

Finally, the same setup as in this study is used in our prior work [20]. In comparison to [20] that uses particle filter [21], however, this proposed strategy uses a data-driven approach that employs deep learning. Although the particle filter algorithm has some advantages such as its high stability with tracking problems and its ability to implicitly track the gain which eliminates the need to have a process model for the gain evolution, it also has its shortcomings. Particularly, its non-deterministic characteristic might lead to wrong predictions when uninformative sensor readings are collected for an extended period. Additionally, its computational intensive requirement (a good filter requires a significant amount of particles) will put quite a burden on the UE. On the contrary, using deep learning puts a less computational load on the UE and its end-to-end characteristic eliminates the need to do feature engineering and makes the classifier system simpler. More importantly, the experimental results in this study confirm that the proposed data-driven approach performs much better than the PF-based strategy used in [20].

Notation: For column vectors, bold lowercase \mathbf{x} is used, bold uppercase \mathbf{X} is used for matrices, and non-bold letters x, X are used for scalars. $[\mathbf{x}]_j$ is the j th entry in a column vector \mathbf{x} . The transpose and conjugate transpose are represented by the superscripts T and $*$, respectively. $\mathcal{N}(\boldsymbol{\mu}, \boldsymbol{\Sigma})$ is a multidimensional Gaussian random variable with mean $\boldsymbol{\mu}$ and covariance $\boldsymbol{\Sigma}$. $\mathcal{U}[a, b]$ is a Uniform random variable with support $[a, b]$. The modulo operator is denoted by the symbol $\text{mod}(\cdot)$. We define $\text{pow2db}(x) = 10 \log_{10}(x)$ and $\text{db2pow}(x) = 10^{\frac{x}{10}}$ functions to transform powers from linear to logarithmic scale and back.

III. SYSTEM MODEL

We consider a communication system shown in Fig. 1 where the RSRP information, i.e., information extracted from beam measurements, as well as orientation information, is used at the UE side for beam prediction.

A. RSRP information

For downlink (DL) BM in 5G NR, the BS sends the beam-formed synchronization signal blocks (SSBs) and/or channel state information reference signals (CSI-RSs). The UE receives the beam-formed transmissions using different receive beams. The UE then reports the index and quality of the best beams to the BS. Subsequently, the BS decides the

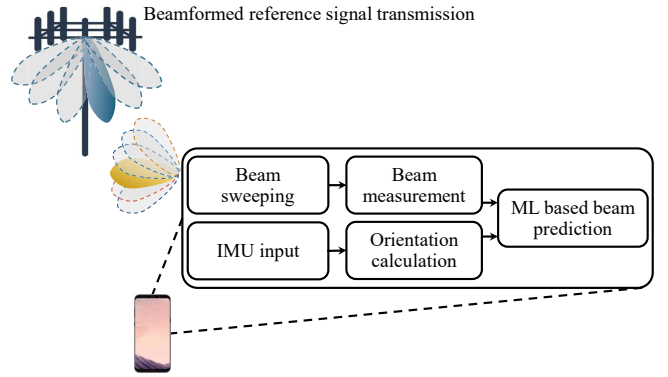
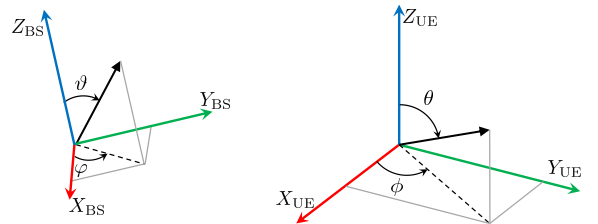


Fig. 1: The block diagram of a BS-UE communication system in which the UE uses beam measurements as well as orientation information for beam prediction.



(a) BS local coordinate system. (b) UE local coordinate system.

Fig. 2: Local coordinate systems of the BS and UE.

best transmit beam. In this work, we consider SSB based DL BM. The transmission power is P_T dBm, and the coordinate systems are shown in Fig. 2. Specifically, the local coordinate system of the BS is shown in Fig. 2a. The transmit beam codebook contains M_{BS} beams. If the BS uses transmit beam $i \in 1, \dots, M_{BS}$, then the transmit beam gain in direction (φ, ϑ) is $F_i(\varphi, \vartheta)$ dB, where φ is the azimuth angle and ϑ is the zenith angle. Similarly, the receive beam code-book contains M_{UE} code-words (or beams), and the local coordinate system used at the UE is shown in Fig. 2b. If the UE uses receive beam $j \in 1, \dots, M_{UE}$, then the receive beam gain in direction (ϕ, θ) is $G_j(\phi, \theta)$ dB, where ϕ is the azimuth angle and θ is the zenith angle.

The SSBs are transmitted with periodicity T_{SS} , and the time variable t denotes the index of an SSB. The received RSRP at time t , i.e., s_t is given as

$$s_t = P_T + \text{pow2db} \left(\frac{\text{SCS}}{\text{BW}} \right) + \text{pow2db} \left(\sum_{c=1}^C \text{db2pow}(p_t^{(c)} + F_{i_t}(\varphi_t^{(c)}, \vartheta_t^{(c)}) + G_{j_t}(\phi_t^{(c)}, \theta_t^{(c)})) \right) + n_t \quad (1)$$

where subcarrier spacing (SCS) is for the SSB, and bandwidth (BW) is for the system, since the RSRP is defined as the average received power over a single sub-carrier. Further, C is the number of multi-paths in the channel, and $p_t^{(c)}$ dB is the path gain of the c -th path at time t . The angle-of-departure (AoD) of the c th path is $(\varphi_t^{(c)}, \vartheta_t^{(c)})$ and the AoA of the c th

path is $(\phi_t^{(c)}, \theta_t^{(c)})$. Finally, i_t is the index of the transmit beam at time t , j_t is the index of the receive beam at time t , $F(\phi, \theta)$ is the BS beam pattern, $G(\phi, \theta)$ is the UE beam pattern, and n_t is the noise.

In this work, we assume the genie-aided knowledge of best transmit beam, i.e., i^* and focus on finding j^* , as our main focus is on the use of UE orientation for BM. Under this assumption, the conventional RSRP-only based BM works in the following manner. An RSRP table $\mathbf{s} \in \mathbb{R}^{M_{\text{UE}} \times 1}$ (with all entries initialized to $-\infty$) is maintained at the UE. The UE receives the SSB through different beams in a round-robin manner. At time t , the j_t -th beam is used as the receive beam, and the j_t -th entry of the RSRP table is subsequently updated as $[\mathbf{s}]_{j_t} = s_t$.

The best receive beam \hat{j}^* can then be bound as $\hat{j}^* = \arg \max_j [\mathbf{s}]_j$. As it takes M_{UE} SSB periods to receive updated RSRP information on all beams, some entries in the RSRP table may be outdated due to temporal changes, e.g., UE orientation.

B. Orientation information

Our objective is to use orientation information coming from an IMU together with the RSRP information for BM as in Fig. 1. The local coordinate system $(X_{\text{UE}}, Y_{\text{UE}}, Z_{\text{UE}})$, and the global coordinate system (X, Y, Z) of the UE are shown in Fig. 3, which are aligned. The rotations around Z , Y , and X are denoted by α , β , and γ respectively [22], and the rotations are assumed in that order [22, Section 7.1]. The rotation matrices around each axis, i.e., $\mathbf{R}_Z(\alpha)$, $\mathbf{R}_Y(\beta)$, and $\mathbf{R}_X(\gamma)$ are defined as

$$\mathbf{R}_Z(\alpha) = \begin{bmatrix} \cos \alpha & -\sin \alpha & 0 \\ \sin \alpha & \cos \alpha & 0 \\ 0 & 0 & 1 \end{bmatrix} \quad (2)$$

$$\mathbf{R}_Y(\beta) = \begin{bmatrix} \cos \beta & 0 & \sin \beta \\ 0 & 1 & 0 \\ -\sin \beta & 0 & \cos \beta \end{bmatrix} \quad (3)$$

$$\mathbf{R}_X(\gamma) = \begin{bmatrix} 1 & 0 & 0 \\ 0 & \cos \gamma & -\sin \gamma \\ 0 & \sin \gamma & \cos \gamma \end{bmatrix} \quad (4)$$

The composite rotation matrix $\mathbf{R}(\alpha, \beta, \gamma)$ is then calculated as

$$\mathbf{R}(\alpha, \beta, \gamma) \triangleq \mathbf{R}_Z(\alpha)\mathbf{R}_Y(\beta)\mathbf{R}_X(\gamma) \quad (5)$$

The UE orientation at time t is determined by α_t , β_t and γ_t . We assume that the UE has access to the erroneous estimates of these orientations, i.e., $\hat{\alpha}_t$, $\hat{\beta}_t$ and $\hat{\gamma}_t$.

IV. SIMULATION SETUP

As the discussion of the data-driven approach merits the discussion of data-set preparation, we first provide the simulation setup, before discussing the data-driven approach. We provide only the most necessary simulation parameters in this article and refer the reader to [20] for the details.

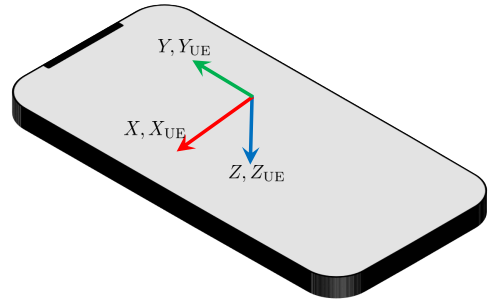


Fig. 3: The orientation of the phone when the UE local coordinate system $X_{\text{UE}}, Y_{\text{UE}}, Z_{\text{UE}}$ is aligned with global coordinate system X, Y, Z .

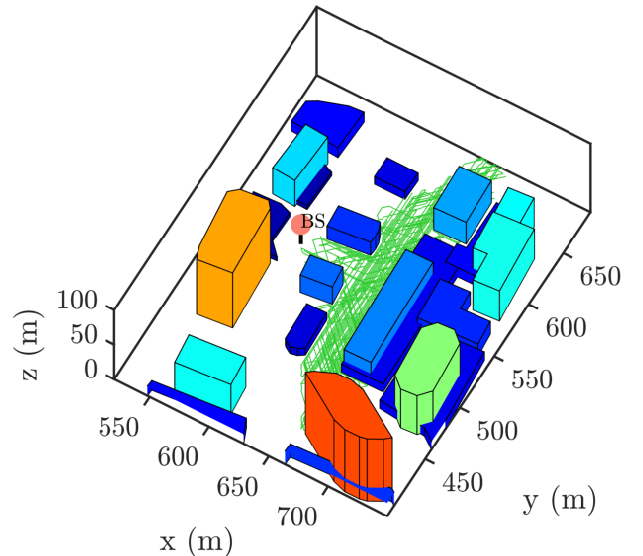


Fig. 4: The ray-tracing simulation setup of downtown Rosslyn, VA. The location of BS is shown with the salmon color disc, and the UE moves along the trajectory shown by green lines.

The ray-tracing channels are generated for downtown Rosslyn, VA, USA, using Wireless InSite® [23] software. In Fig. 4, the BS is shown with a salmon color disc. The UE trajectory is shown via green colored lines. For generating the trajectory, the UE picks a random destination point in the cell, and once it reaches the picked point, it picks another random destination point. The A* search algorithm is used to find a short route from one randomly picked destination point to the next [24]. The UE trajectory is limited to a 120° sector, and for the simulation, the UE picks 200 random destination points, and the total length of the trajectory is 20 km.

The operating frequency is 28 GHz, BW is 100 MHz, SCS is 240 kHz, and the transmit power is $P_T = 30$ dBm. As our main focus is BM at the UE side, we assume a single isotropic antenna BS, i.e., $M_{\text{BS}} = 1$. The UE either uses $M_{\text{UE}}^{\text{W}} = 8$ wide beams or $M_{\text{UE}}^{\text{N}} = 28$ narrow beams. The codebooks are obtained using the K-Means method of [25]. The codebooks are designed assuming 3 bit phase-shifters with no amplitude

TABLE I: The four cases with slow or fast rotation speed, normal or sporadic RSRPs information, and smooth or non-smooth rotation.

Case	Rotation speed (σ)	RSRP information rate (f)	Rotation smoothness (K)
1	Slow (1°)	Normal (1)	Smooth (21)
2	Fast (10°)	Normal (1)	Smooth (21)
3	Fast (10°)	Sporadic (3)	Smooth (21)
4	Fast (10°)	Sporadic (3)	Non-smooth (5)

scaling. Fig. 5 shows the 3 dB contour plots of the wide and narrow beams. From beam measurements on a mobile device, it was observed that the measured RSRP varies substantially over time, even in a static setup. We use the method discussed in [20] to generate the noise n_t that models this variation.

We consider a filtered random walk based UE orientation model. Specifically, consider a random walk $\bar{\alpha}_t = \bar{\alpha}_{t-1} + \mathcal{N}(0, \sigma^2)$ where $\bar{\alpha}_0 \sim \mathcal{U}[0^\circ, 360^\circ]$. Then, the filtered random walk is $\alpha_t = \frac{1}{K} \sum_{k=0}^{K-1} \bar{\alpha}_{t-k}$ where K is the filter length. A large value of σ implies fast rotation, and a large K implies smooth variation. The same procedure is followed for generating α_t , β_t , and γ_t , and also a same value of σ is used. We model the IMU error as zero mean white Gaussian [26]. The level of error in each axis is then determined by the standard deviation, i.e., $\sigma_\alpha = 2^\circ$, $\sigma_\beta = 1^\circ$ and $\sigma_\gamma = 1^\circ$.

We create four test cases shown in Table I to concretely capture the different levels of rotation speed, RSRP information rates, and orientation smoothness. The rotation speed is either ‘‘Slow’’, i.e., $\sigma = 1^\circ$ per 20 ms, or ‘‘Fast’’, i.e., $\sigma = 10^\circ$ per 20 ms. The RSRP information rate is either ‘‘Normal’’, i.e., $f = 1$ and we get an RSRP measurement every T_{SS} , or ‘‘Sporadic’’, i.e., $f = 3$ and we get an RSRP measurement every $3T_{SS} = 60$ ms. The rotation is either ‘‘Smooth’’, i.e., $K = 21$, or ‘‘Non-smooth’’, i.e., $K = 5$. Finally, a higher case index is a more favorable scenario for orientation-information use.

V. DATA-DRIVEN BEAM MANAGEMENT

We divide the discussion of the data-driven BM into two parts. First, we discuss the data preparation and partition, and then we discuss in detail the deep learning approach that is used for our BM solution.

A. Data preparation and partition

In order to use both RSRP and IMU information, the data from these sensors need to be processed and fused together. For the RSRP information, note that the UE receives the SSB by varying the receive beams in a round-robin manner¹. Specifically, the beam index of the beam used at time t is $j_t = \text{mod}(\frac{t}{f}, M_{UE}) + 1 \in \{1, \dots, M_{UE}\}$ when t is an integer multiple of f ($f = 1$ or 3 in the simulation), and the RSRP measured on the beam j_t is s_{j_t} . To prepare the data for the RNN, an $M_{UE} \times 1$ vector is created with the j_t th entry set to s_{j_t} , and all the other entries set to 0. For the normal measurement mode, a new RSRP corresponding to an updated

¹In this paper, we do not consider the scenario where the UE changes the receive beam sweeping order. However, as long as the same beam sweeping order is adopted in the training and operation phases, our RNN is applicable.

j_t is available for every t , and the updated $1 \times M_{UE}$ vector is fed to the RNN. For sporadic measurement mode, the $1 \times M_{UE}$ vector at each time step, no matter it is updated or not, is fed to the RNN. For the IMU information a new measurement is available every time step regardless of the RSRP information rate. The IMU information is captured directly through the matrix $\mathbf{R}(\alpha, \beta, \gamma)$ discussed in Section III-B. This 3×3 rotation matrix is flattened to get a 1×9 vector. Therefore, after concatenation, the RSRP information vector $1 \times M_{UE}$ and rotation vector 1×9 , make a $1 \times (M_{UE} + 9)$ input vector for the RNN. The output at each time step is the one hot encoded best beam index \hat{j}^* .

Three UE movement speeds were used, i.e., 20 km h^{-1} , 60 km h^{-1} , and 100 km h^{-1} . For each speed, we wanted to have around a million data points. As the number of sample points on the 20 km trajectory with sampling interval 20 ms are around 180,000 for UE speed of 20 km h^{-1} , we used 6 independent realizations of the orientation to get around a million points. Similarly for 60 km h^{-1} and 100 km h^{-1} , we needed around 17 and 28 independent realizations of the orientation to get around a million points. Note that the UE rotation speed (either 1° or 10° per 20 ms) is independent of the UE movement speed.

We partitioned the data across the trajectory. This implied that there was a high chance of having wireless channels in the testing set that were not seen by the RNN through the training set. The training, validating, and test data split is around 70%, 20%, and 10%. Note that we have data for three different UE speeds, two different rotation speeds, two different RSRP information rates, and two levels of smoothness. We combine all this data to increase the training data size for RNN.

B. The deep learning approach

To handle the BM problem in a data-driven manner, we utilized supervised deep learning. We designed and used a RNN architecture to perform beam prediction. Since this is a time-series classification problem, using RNN is logical as RNN exhibits temporal dynamic behavior which allows it to learn and process the temporal relation in the input sequences. Our RNN architecture is shown in Fig. 6. We used this architecture because it yielded the best results and it is relatively lightweight. The architecture includes a LSTM cell [27] with a hidden size of 128 neurons. This is followed by a fully connected (FC) layer of size $2 \times M_{UE}$ with a ReLU activation and another FC layer of size M_{UE} with a soft-max activation for multi-class classification purpose.

The RNN adopts the categorical cross-entropy loss function. Specifically, the loss L_t at each time step t is calculated as

$$L_t = - \sum_{m=1}^{M_{UE}} y_{t,m} \log(\hat{y}_{t,m}) \quad (6)$$

where $y_{t,m}$ is the corresponding target value at time step t of class m , and $\hat{y}_{t,m}$ is the predicted probability of class m at time t . Additionally, Adam optimizer with a learning rate of 0.001 was used. The training took 10,000 epochs to converge with a batch size of 6 trajectories (sequences).

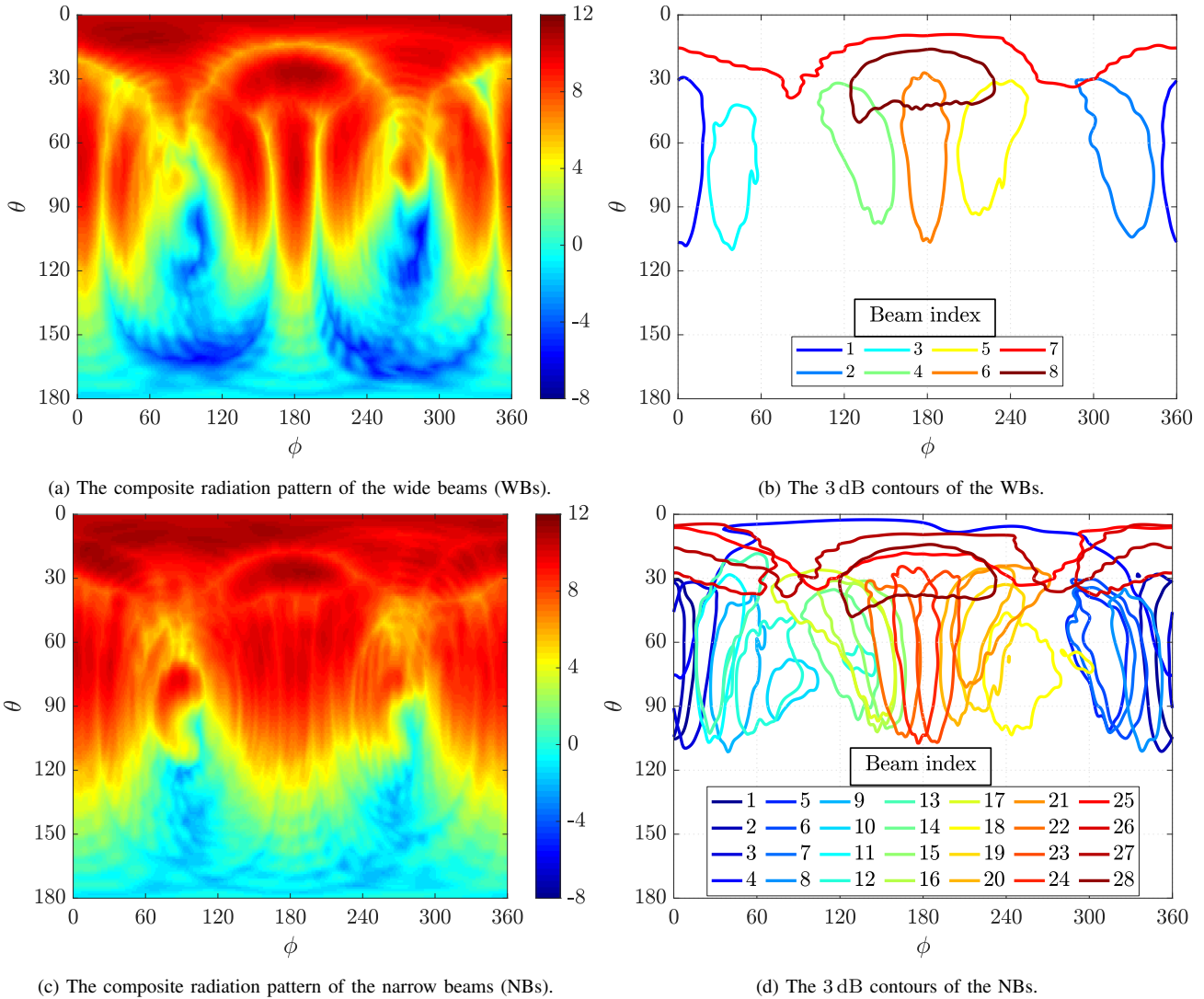


Fig. 5: The composite radiation patterns 3 dB contours of the $M_{UE}^W = 8$ WBs and $M_{UE}^N = 28$ NBs. The composite radiation pattern is plotted in the dB scale and the beam indices for the contour plots are given in the legend. They are based on a realistic phone setup with three 1×4 ULA arrays on the left edge, right edge and the back of the phone, respectively.

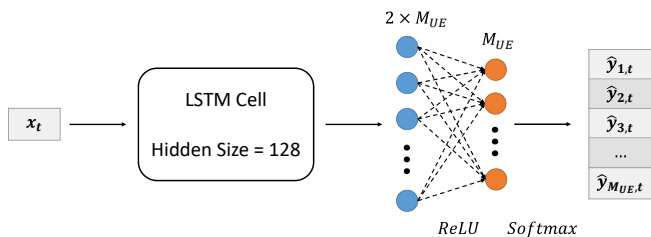


Fig. 6: The RNN architecture consists of a LSTM cell and two FC layers, where x_t (size: $1 \times (M_{UE} + 9)$) is the input and \hat{y}_t (size: $1 \times M_{UE}$) is the beam prediction at time t .

In the inference step, full trajectories (time sequences) were fed into the RNN. At each time step t within a trajectory, a beam decision will be produced. Fig. 7 describes the training and inference process. The input at each step consist of 2

components. The first component is an array \mathbf{T}_t of size M_{UE} with the RSRP value of the last measured beam is set at that beam index i and the values at other indices are set to 0. The second component is the rotation matrix computed from the current IMU orientation \mathbf{R}_t . The output at each time step is \hat{y}_t which is the beam index of the best beam in the form of a one hot encoded vector. Additionally, the hidden state of the LSTM cell h_t at each time step is also returned to re-fed into the RNN.

VI. SIMULATION RESULTS

We now present the simulation results that show the supremacy of the proposed data-driven strategy compared to conventional BM and PF based BM strategy of [20]. For this purpose, we use three metrics as follows.

TABLE II: The performance comparison of orientation-assisted BM strategies (PF is Particle Filter and RNN is Recurrent Neural Network) in comparison with RSRP-only BM in terms of beam prediction accuracy (%), mean RSRP (dBm), and RSRP loss (dB). The performance is compared for two different UE movement speeds and four cases outlined in Table I.

Case			1			2			3			4		
Metric			AC	RSRP	Loss									
20 km h ⁻¹	WB	RSRP-only	90.16	-101.9	0.17	75.60	-102.57	0.83	49.10	-104.91	3.17	40.43	-105.90	4.15
		PF	73.42	-102.57	0.84	70.65	-102.84	1.10	54.80	-104.53	2.78	50.58	-104.97	3.22
		RNN	88.88	-101.9	0.17	80.71	-102.22	0.47	80.71	-102.22	0.47	60.45	-103.69	1.93
	NB	RSRP-only	63.49	-100.98	0.86	28.55	-104.51	4.42	13.11	-107.63	7.54	11.14	-108.04	7.94
		PF	37.14	-102.99	2.87	33.05	-103.38	3.29	21.72	-105.56	5.47	21.41	-105.66	5.57
		RNN	57.52	-101.02	0.90	43.99	-101.98	1.88	30.08	-103.51	3.42	26.69	-103.99	3.90
60 km h ⁻¹	WB	RSRP-only	85.36	-102.59	0.41	72.20	-103.06	1.09	44.16	-105.65	3.68	36.87	-106.53	4.56
		PF	69.06	-103.36	1.18	67.83	-103.30	1.33	49.75	-105.28	3.31	47.19	-105.56	3.60
		RNN	84.53	-102.55	0.36	78.18	-102.63	0.64	78.18	-102.63	0.64	57.09	-104.24	2.26
	NB	RSRP-only	53.39	-102.21	1.76	26.36	-105.10	4.84	10.74	-108.33	8.07	9.53	-108.73	8.43
		PF	31.62	-103.93	3.48	30.31	-103.95	3.69	18.73	-106.46	6.20	18.34	-106.50	6.20
		RNN	51.58	-101.91	1.44	41.35	-102.47	2.20	28.03	-104.10	3.84	25.40	-104.53	4.22
100 km h ⁻¹	WB	RSRP-only	81.07	-102.43	0.66	69.31	-103.22	1.30	41.12	-106.03	4.11	34.52	-106.78	4.86
		PF	67.46	-103.12	1.35	65.03	-103.52	1.60	45.29	-105.76	3.84	42.98	-106.02	4.10
		RNN	80.65	-102.34	0.54	74.36	-102.80	0.86	74.36	-102.80	0.86	52.33	-104.68	2.74
	NB	RSRP-only	46.73	-102.66	2.47	23.86	-105.60	5.26	9.88	-108.52	8.17	9.45	-108.86	8.48
		PF	29.24	-104.28	4.09	27.79	-104.64	4.30	17.00	-106.97	6.63	15.98	-107.14	6.76
		RNN	45.38	-102.11	1.89	37.09	-103.00	2.64	25.02	-104.69	4.33	23.07	-105.08	4.68

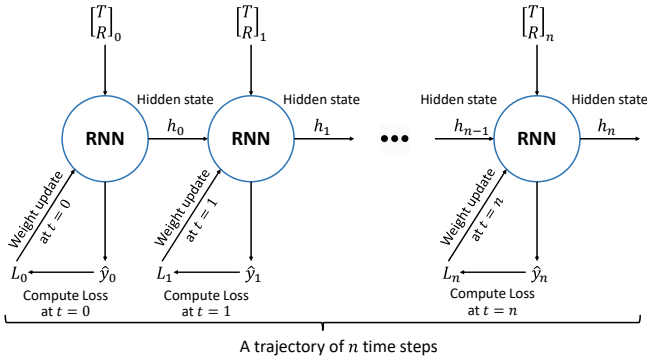


Fig. 7: The training and inference step. For the training step, at each time step t , the input $[\mathbf{T}, \mathbf{R}]_t$ is fed into the RNN. A beam decision \hat{y}_t will be produced. The loss L_t shall then be calculated and used to update the RNN. For the inference step, the process stops at the beam decision.

- 1) Beam prediction accuracy or “AC” is the percentage of times the beam-predicted by a practical strategy, e.g., “RSRP-only” or ‘Orientation-assisted” is the same as the “genie-aided” best beam. The “genie-aided” best beam is obtained assuming instantaneous RSRP knowledge of all the beams at the UE
- 2) The mean RSRP or “RSRP”.
- 3) “RSRP loss” or “Loss” is obtained by subtracting the RSRP of a predicted beam from the RSRP of the genie-aided best beam and taking the mean of the difference.

From the results in Table II, we see that for Case 1, the accuracy and the mean RSRP of the orientation-assisted classical signal processing method, i.e., PF strategy in [20], is lower compared to RSRP-only. This is because Case 1 is not

a favorable scenario for the use of orientation information. Specifically, the rotation speed itself is slow so there is not much benefit of using rotation information. In other words, before the mobile significantly rotates, RSRP information on all (or most) beams can be collected to maintain relatively good BM. Further, as the orientation information is erroneous, using orientation information can harm BM. Even in this unfavorable case for the signal processing approach, the proposed machine learning method, i.e, deep learning strategy, can still work. Although the accuracy is a slightly lower than that of RSRP-only, the mean RSRP, which is a relevant metric for the communication, is very close or even better than RSRP-only.

In Case 2, the RNN performs better than the RSRP-only, whereas the PF does not. In Case 3 and 4 the RSRP information rate is lower than the orientation information rate and the benefit of using the orientation-assisted strategies for BM becomes clear. We can see that depending on the user movement speed and orientation smoothness, using orientation-assisted strategies can improve the beam prediction accuracy significantly. For example, at (Case 3, 60 km h⁻¹, WB), the accuracy increases by 34% from 44.16% to 78.18%. The mean RSRP is also boosted. For example, at (Case 4, 60 km h⁻¹, NB), the mean RSRP improves by 4.2 dB from -108.73 dBm to -104.53 dBm.

Finally, note that the performance of the proposed deep learning strategy is consistently better than the PF strategy across all the scenarios. Moreover, the complexity of the deep learning strategy in terms of run-time cost is better in our experiments. The PF strategy uses 1000 particles to track the angle of arrival in the local coordinate system and updates their next values at each time step which might be problematic in terms of latency requirement. On the other hand, the deep learning strategy, although needs a large training overhead, is

very efficient for online beam prediction. Our approach has the potential to be used in more general scenarios besides our experiment given that a larger and more diverse dataset is provided for the training purpose. Additionally, transfer learning [28] as well as meta learning [29] can also be used to quickly adjust the model to satisfy the requirement of the changing problem.

VII. CONCLUSION

We proposed a data-driven BM strategy that jointly utilizes the RSRP and orientation information through an RNN. Specifically, we formulated the BM problem as a classification problem where one class stands for a beam. The proposed strategy outperforms the conventional BM which relies only on the RSRP measurement. In particular, the data-driven strategy can improve BM accuracy by 34% and boost the mean RSRP by 4.2 dB in challenging environments of high mobility and fast rotation UE and sporadic RSRP measurement. The 4.2 dB gain is significant at the UE because it is equivalent to a cut of uplink transmission power by 62%, which substantially improves the UE battery life. Furthermore, when both RSRP measurement and orientation information are utilized, the data-driven strategy performs consistently better than the model-based PF strategy. Lastly, the high-complexity RNN training is done offline, and the data-driven strategy is more efficient than PF for online BM.

The training of the RNN is done with the simulation data of a single deployment area in the downtown area. More training data from other deployment areas, for example, suburban, rural, can be obtained from simulation and used to train a more robust RNN for different propagation environments. This is left for future work. Another future direction is to implement and evaluate the proposed strategy in a mobile device. The 5G mmWave devices may have a different number of mmWave antenna arrays and mount them in different locations, thus the WB and NB radiation patterns will be different. Considering such kind of difference between the simulation and real deployment, training of the RNN with more simulation data and possibly field measurement data, would be needed.

REFERENCES

- [1] T. S. Rappaport, S. Sun, R. Mayzus, H. Zhao, Y. Azar, K. Wang, G. N. Wong, J. K. Schulz, M. Samimi, and F. Gutierrez, "Millimeter wave mobile communications for 5g cellular: It will work!" *IEEE access*, vol. 1, pp. 335–349, 2013.
- [2] M. Giordani, M. Polese, M. Mezzavilla, S. Rangan, and M. Zorzi, "Toward 6g networks: Use cases and technologies," *IEEE Communications Magazine*, vol. 58, no. 3, pp. 55–61, 2020.
- [3] E. Bjornson, L. Van der Perre, S. Buzzi, and E. G. Larsson, "Massive MIMO in sub-6 GHz and mmWave: Physical, practical, and use-case differences," *IEEE Wireless Communications*, vol. 26, no. 2, pp. 100–108, 2019.
- [4] M. Giordani, M. Polese, A. Roy, D. Castor, and M. Zorzi, "A tutorial on beam management for 3GPP nr at mmwave frequencies," *IEEE Communications Surveys Tutorials*, vol. 21, no. 1, pp. 173–196, 2019.
- [5] Y.-N. R. Li, B. Gao, X. Zhang, and K. Huang, "Beam management in millimeter-wave communications for 5G and beyond," *IEEE Access*, vol. 8, pp. 13 282–13 293, 2020.
- [6] Y. Heng, J. G. Andrews, J. Mo, V. Va, A. Ali, B. L. Ng, and J. C. Zhang, "Six key challenges for beam management in 5.5G and 6G systems," *IEEE Communications Magazine*, vol. 59, no. 7, pp. 74–79, 2021.
- [7] V. Va, J. Choi, T. Shimizu, G. Bansal, and R. W. Heath, "Inverse multipath fingerprinting for millimeter wave V2I beam alignment," *IEEE TVT*, vol. 67, no. 5, pp. 4042–4058, 2018.
- [8] F. Maschiatti, D. Gesbert, P. de Kerret, and H. Wymeersch, "Robust location-aided beam alignment in millimeter wave massive MIMO," in *GLOBECOM 2017 - 2017 IEEE Global Communications Conference*, 2017, pp. 1–6.
- [9] Y. Heng and J. G. Andrews, "Machine learning-assisted beam alignment for mmWave systems," *IEEE TCCN*, vol. 7, no. 4, pp. 1142–1155, 2021.
- [10] A. Ali, N. Gonzalez-Prelcic, and R. W. Heath, "Millimeter wave beam-selection using out-of-band spatial information," *IEEE-J-WCOM*, vol. 17, no. 2, pp. 1038–1052, 2017.
- [11] M. Alrabeiah and A. Alkhateeb, "Deep learning for mmwave beam and blockage prediction using sub-6 GHz channels," *IEEE Transactions on Communications*, vol. 68, no. 9, pp. 5504–5518, 2020.
- [12] A. Ö. Kaya and H. Viswanathan, "Deep learning-based predictive beam management for 5G mmwave systems," in *2021 IEEE WCNC*. IEEE, 2021, pp. 1–7.
- [13] S. H. Lim, S. Kim, B. Shim, and J. W. Choi, "Deep learning-based beam tracking for millimeter-wave communications under mobility," *IEEE Transactions on Communications*, vol. 69, no. 11, pp. 7458–7469, 2021.
- [14] H. Echigo, Y. Cao, M. Bouazizi, and T. Ohtsuki, "A deep learning-based low overhead beam selection in mmWave communications," *IEEE TVT*, vol. 70, no. 1, pp. 682–691, 2021.
- [15] K. Ma, D. He, H. Sun, Z. Wang, and S. Chen, "Deep learning assisted calibrated beam training for millimeter-wave communication systems," *IEEE Transactions on Communications*, vol. 69, no. 10, pp. 6706–6721, 2021.
- [16] D.-S. Shim, C.-K. Yang, J. H. Kim, J. P. Han, and Y. S. Cho, "Application of motion sensors for beam-tracking of mobile stations in mmwave communication systems," *Sensors*, vol. 14, no. 10, pp. 19 622–19 638, 2014.
- [17] Z. Qi and W. Liu, "Three-dimensional millimetre-wave beam tracking based on smart phone sensor measurements and direction of arrival/time of arrival estimation for 5g networks," *IET Microwaves, Antennas & Propagation*, vol. 12, no. 3, pp. 271–279, 2018.
- [18] M. Brambilla, M. Nicoli, S. Savaresi, and U. Spagnolini, "Inertial sensor aided mmwave beam tracking to support cooperative autonomous driving," in *2019 IEEE ICC Workshops*. IEEE, 2019, pp. 1–6.
- [19] S. Rezaie, C. N. Manchón, and E. De Carvalho, "Location-and Orientation-Aided Millimeter Wave Beam Selection Using Deep Learning," in *2020 IEEE International Conference on Communications, ICC 2020*, 2020, pp. 1–6.
- [20] A. Ali, J. Mo, B. L. Ng, V. Va, and J. C. Zhang, "Orientation-assisted beam management for beyond 5g systems," *IEEE Access*, vol. 9, pp. 51 832–51 846, 2021.
- [21] H. R. Künsch, "Particle filters," *Bernoulli*, vol. 19, no. 4, pp. 1391–1403, 2013.
- [22] 3GPP, "Study on channel model for frequencies from 0.5 to 100 GHz," 3rd Generation Partnership Project (3GPP), TR 38.901, Dec. 2017, version 14.3.0. [Online]. Available: <http://www.3gpp.org/DynaReport/38901.htm>
- [23] Remcom Inc., *Wireless InSite 3.3.5 Reference Manual*, November 2020.
- [24] P. E. Hart, N. J. Nilsson, and B. Raphael, "A formal basis for the heuristic determination of minimum cost paths," *IEEE transactions on Systems Science and Cybernetics*, vol. 4, no. 2, pp. 100–107, 1968.
- [25] J. Mo, B. L. Ng, S. Chang, P. Huang, M. N. Kulkarni, A. Alammouri, J. C. Zhang, J. Lee, and W.-J. Choi, "Beam codebook design for 5g mmwave terminals," *IEEE Access*, vol. 7, pp. 98 387–98 404, 2019.
- [26] M. Kok, J. D. Hol, and T. B. Schön, "Using inertial sensors for position and orientation estimation," *arXiv preprint arXiv:1704.06053*, 2017.
- [27] S. Hochreiter and J. Schmidhuber, "Long short-term memory," *Neural computation*, vol. 9, no. 8, pp. 1735–1780, 1997.
- [28] C. Tan, F. Sun, T. Kong, W. Zhang, C. Yang, and C. Liu, "A survey on deep transfer learning," in *ICANN*. Springer, 2018, pp. 270–279.
- [29] W.-Y. Chen, Y.-C. Liu, Z. Kira, Y.-C. F. Wang, and J.-B. Huang, "A closer look at few-shot classification," *arXiv preprint arXiv:1904.04232*, 2019.